UTe_2: A nearly insulating half-filled $j = \frac{5}{2}$ $5f^3$ heavy-fermion metal

Alexander B. Shick*
Institute of Physics, Czech Academy of Science, Na Slovance 2, CZ-18221 Prague, Czech Republic

Shin-ichi Fujimori
Materials Sciences Research Center, Japan Atomic Energy Agency, Sayo, Hyogo 679-5148, Japan

Warren E. Pickett†
Department of Physics, University of California, Davis, California 95616, USA

(Received 27 September 2020; accepted 22 February 2021; published 16 March 2021)

Correlated band theory implemented as a combination of density functional theory with exact diagonalization [DFT + U(ED)] of the Anderson impurity term with Coulomb repulsion U in the open 14-orbital $5f$ shell is applied to UTe_2. The small gap for $U = 0$, evidence of the half-filled $j = \frac{5}{2}$ subshell of $5f^3$ uranium, is converted for $U = 3$ eV to a flat-band semimetal with small heavy-carrier Fermi surfaces that will make properties sensitive to pressure, magnetic field, and off-stoichiometry, as observed experimentally. Two means of identification from the Green's function give a mass enhancement of the order of 12 for already heavy (flat) bands, consistent with the common heavy-fermion characterization of UTe_2. The predicted Kondo temperature around 100 K matches the experimental values from resistivity. The electric field gradients for the two Te sites are calculated by DFT + U(ED) to differ by a factor of 7, indicating a strong site distinction, while the anisotropy factor $\eta = 0.18$ is similar for all three sites. The calculated uranium moment $\langle M^2 \rangle^{1/2}$ of 3.5 μ_B is roughly consistent with the published experimental Curie-Weiss values of 2.8 and 3.3 μ_B (which are field-direction dependent), and the calculated separate spin and orbital moments are remarkably similar to Hund's rule values for an f^3 ion. The $U = 3$ eV spectral density is compared with angle-integrated and angle-resolved photoemission spectra, with agreement that there is strong $5f$ character at, and for several hundred meV below, the Fermi energy. Our results support the picture that the underlying ground state of UTe_2 is that of a half-filled $j = \frac{5}{2}$ subshell with two half-filled $m_j = \pm\frac{1}{2}$ orbitals forming a narrow gap by hybridization and then driven to a conducting state by configuration mixing (spin-charge fluctuations). UTe_2 displays similarities to UPt_3 with its $5f$-dominated Fermi surfaces rather than a strongly localized Kondo lattice system.

DOI: 10.1103/PhysRevB.103.125136

I. INTRODUCTION

Recently discovered superconductivity (SC) in the heavy-fermion material UTe_2 [1,2] below 1.7 K, earlier studied in single-crystal form [3], shows a number of peculiar aspects. Unlike in several other U superconductors (UGe_2, UCoGe, URhGe, and UCoAl) which display coexisting superconductivity and ferromagnetism, no long-range magnetic order in the ground state has been observed. The magnetic susceptibility [1,2] has Curie-Weiss character, with magnetic moment in the 2.8−3.3 μ_B/U range. Magnetic moments in a metal that do not order suggest that UTe_2 is associated with a class of conducting spin liquids. The large and anisotropic Curie-Weiss magnetic susceptibility suggests antiferromagnetic coupling, whereas other probes [NMR Knight shift and spin-lattice relaxation rate $(1/TT_1)$] suggest critical ferromagnetic fluctuations that could mediate SC in UTe_2 [1,2,4]. The phase diagrams versus field and its direction, temperature, and pressure—including reentrant superconductivity with application of field—are unusually complex, but those complications will not be addressed in this paper.

UTe_2 is, however, a heavy-fermion metal, with a large Sommerfeld coefficient $\gamma \approx 120$ mJ/K^2 [1,2], indicative of Kondo screening of local moments. The resistivity $\rho \sim 1$ mΩ cm slowly increases from room temperature down to 75 K, and then it decreases rapidly over two orders of magnitude just above T_c, typical heavy-fermion (HF) behavior with a Kondo temperature of ∼100 K [1]. The susceptibility for the field along the easy a axis increases strongly below 100 K, becoming a factor of 5 or more larger than in the other two directions. The interpretation has been that of critical magnetic fluctuations around incipient ferromagnetic (FM) order along the a axis. A considerable number of measurements of electrical and thermal conductivity, NMR spectra, and penetration depth in magnetic fields gives strong justification of a point-node, Weyl superconducting state.

Based on a nonvanishing specific heat coefficient C_v/T below T_c, UTe_2 had originally been suggested by Ran *et al.* [5] to provide a new phase of superconducting matter with a "Bogoliubov Fermi surface," a Fermi surface that is gapless

*shick@fzu.cz
†pickett@physics.ucdavis.edu

over not points, or lines, but an area. However, subsequent extension of the measurements to 50 mK revealed an *upturn* in C_v/T. The normal state C_v (i.e., above the critical magnetic field) was fit with the conventional form augmented by a residual contribution C_x of unknown origin, modeled by a $C_x/T = A_{\rm div}T^{-1/3}$ form in the region of 50 mK to T_c. C_x would arise from thermal excitations that are not gapped by SC [1,2,6]. Supposing that this extrapolation is reasonable up to around 2 K (taken literally, it would give a divergent entropy), the excess entropy is (we estimate) of the order of $S_x \sim \alpha_x k_B \ln 2$, with $\alpha_x \sim 10^{-2}$, small enough to be extrinsic in origin.

U-based compounds provide a spectacular variety of behaviors, from ground states to unusual spectra. The ferromagnetic superconductors mentioned above have been reviewed and compared by Aoki, Ishida, and Flouquet [7]. These compounds seem to require correlation corrections beyond conventional density functional theory (DFT) in its local or semilocal approximations to account for their properties. Superconducting UPt_3 ($T_c < 1$ K), on the other hand, has six complicated Fermi surfaces that are described quite well by DFT calculations [8,9], with excellent agreement requiring only energy shifts of a few tens of meV. Isovalent and isostructural UPd_3, on the other hand, is reproduced only when the U $5f$ states are localized (removed from the valence states) [10].

The electronic structure of UTe_2 has been studied from a first-principles itinerant [local density approximation (LDA)] viewpoint making use of DFT, initially by Aoki *et al.* [2] and Fujimori *et al.* [11]. LDA, however, predicts a small gap for this heavy-fermion metal, so these works were followed by others which have incorporated some correlation correction related to a (semi)localized nature of the $5f$ states. Two of the current authors applied a DFT + orbital polarization approach [DFT + U(OP), using a Coulomb repulsion $U = J$], obtaining heavy $5f$ bands giving large Fermi surfaces (FSs) [12]. In these calculations the uranium $5f$ states are treated as basically itinerant, with the repulsion U and Hund's exchange J_H encouraging orbital polarization. Analysis indicated two roughly half-filled $5f$ orbitals, $m_j = \pm\frac{1}{2}$, at the Fermi level, suggesting multiband half-filled physics.

Some of the most basic theoretical questions are unsettled. Standard DFT calculations give a U $5f$ occupation near f^3. From the viewpoint of strongly localized $5f$ orbitals ($U = 6$ eV), Miao *et al.* investigated the effect of removing the $5f$ states from consideration, i.e., using $ThTe_2$ without $5f$ occupation as an underlying model of Fermi level bands [13]. Applying dynamical mean-field theory (DFT+DMFT) to UTe_2 with a large value of repulsion U (with similar results obtained by Xu *et al.* [14]), the $5f$ bands were shifted in Mott insulator fashion away from E_F, leaving a dispersive Te band and a large Fermi surface that was supported by their angle-resolved photoemission spectroscopy (ARPES) spectra. A similar shift of $5f$ bands was observed by Ishizuka *et al.* [15] applying the DFT + U method, even for moderate values of U in the 1–2-eV range. ARPES data taken at higher energy with longer escape depth, however, give clear evidence of strong $5f$ character extending to E_F [11]. Both the DFT + U and DFT+DMFT methods predict a predominant $5f^2$ configuration (our own DFT + U calculations do so as well), whereas uranium core level spectroscopy [16] indicates that the $5f^3$ configuration is dominant, as in several other itinerant uranium intermetallics. We will present evidence that supports a dominant f^3 configuration. We address these differences within this paper, with some emphasis on angle-integrated photoemission spectroscopy (AIPES).

Less strongly correlated methods, such as we will present, leave flat $5f$ bands at E_F in a hybridized band picture consistent with $5f$-dominated Fermi surfaces and with AIPES data, whereas transport and thermodynamic properties will be enhanced by residual (dynamic) interactions. Note that some U compounds, for example, UPt_3 and UBe_{13}, are also heavy-fermion metals that do not order magnetically but display exotic superconducting gap symmetry and $5f$-electron-dominated Fermi surfaces [7].

This itinerant-localized dichotomy is itself not so unusual in metallic actinide compounds, reflecting the "dual" nature [17] often exhibited by open $5f$ shells. Early on, Hill recognized the shortest U-U separation as a critical parameter in uranium intermetallics and provided the "Hill plot" [18,19] of ordering temperature (magnetic or superconducting) versus U-U separation. If shorter than 3.5 Å, the $5f$ states are itinerant and sometimes superconducting; if longer, they display a local moment and usually order. This critical separation is not absolute: The Hill criterion was found to be violated when the heavy-fermion metals UPt_3 and UBe_{13} were synthesized and found to be superconducting without magnetic order. Still, the Hill criterion is a very useful and physically motivated guide. In this picture, the nearest-neighbor U-U separation in UTe_2 of 3.78 Å puts it well into the localized regime of the Hill plot: magnetic rather than superconducting. Just how UTe_2 violates the Hill criterion is a fundamental question in the understanding of this fascinating compound.

This dual nature of the $5f$ shell requires that both local and itinerant features of the f electrons may need to be allowed in a description of the electronic structure of UTe_2. Ishizuka *et al.* [15] performed DFT + U calculations [related somewhat to the DFT + U(OP) results mentioned above] for empirically reasonable values of the effective Coulomb $U_{\rm eff} = U - J =$ 1.1–2.0 eV, $J = 0$. Constraining their DFT + U calculations to the nonmagnetic phase, they obtained a metallic band structure, with reconstruction occurring around $U \sim$ 1.1 eV. Contrary to the results of Refs. [13,14], the electronic states near the Fermi energy E_F formed narrow bands with predominantly $5f$ character. The fundamental limitation of these calculations is that they rely on a single-determinant approximation for the $5f$ manifold of the U atom, and the DFT + U method is more adept in describing occurrence and effects of long-range magnetic order. Our calculations parallel to those of Ishizuka *et al.* indicate that their choice of Hund's exchange $J = 0$, which neglects the anisotropy $U_{m,m'}$ of the repulsive interaction and misses Hund's exchange, has a substantial effect of the resulting band structure.

In this paper we study electron correlation effects in UTe_2 beyond the static mean-field DFT + U approximation. We extend the DFT method making use of an Anderson impurity treatment of the $5f$ shell treated with exact diagonalization (ED) techniques and including the full self-consistency over the charge density. In Sec. II we describe the basic equations of the DFT + U(ED) method. In Sec. III the electronic

structure results for a conventional value of Coulomb $U =$ 3 eV are presented and compared with large Coulomb $U =$ 6 eV results. Section IV is devoted to a comparison with photoemission results, and a summary in Sec. V concludes the paper.

II. STRUCTURE AND METHODS

A. Structure

UTe_2 crystallizes in a body-centered orthorhombic *Immm* structure [3] (space group No. 71) with $a = 4.161$ Å, $b =$ 6.122 Å, and $c = 13.955$ Å, this volume containing two formula units (f.u.) [see Fig. 1(a)]. The atomic sites and symmetries are as follows: U, (0,0,0.13544) 4*i* *mm*2; Te1, $(\frac{1}{2}, 0, 0.2975)$ 4*j* *mm*2; and Te2, $(0, 0.2509, \frac{1}{2})$ 4*h* *m*2*m*. The U-U separations are, in increasing order, 3.78 Å dimer separations directed along the *c* axis, 4.16 Å along the *a* axis (the lattice constant), 4.89 Å in the *b*-*c* plane, and 6.12 Å along the *b* axis (the lattice constant). The normal to the cleavage plane lies 23.7° from the *b* axis in the *b*-*c* plane. The structure is sometimes pictured as U ladders lying in the cleavage plane, or even two sets of U ladders, but the large U-U separation makes any quasi-one-dimensional aspects difficult to identify. Note that much of our description will use the orthorhombic pseudozone with dimensions $\frac{2\pi}{a}, \frac{2\pi}{b}, \frac{2\pi}{c}$.

B. Formalism of the DFT + *U*(ED) method

Given the combination of itinerant behavior with localized physics in actinide materials and the Fermi liquid character of UTe_2, we aim for an effective (low energy) band structure that nevertheless includes essential effects of on-site repulsion and Hund's exchange on the uranium site and related configurations and does so self-consistently. We use an extension of the widely used DFT + U method [20] that makes use of a combination of DFT with the exact diagonalization (ED) of the multiconfigurational $5f$ shell of uranium, in the spirit of a generalized and orbital-occupation (charge, with spin) self-consistent generalization of the Anderson impurity model analogous to that done in dynamical mean-field theory.

This DFT + U(ED) method takes advantage of the fact that electron interactions in the *s*, *p*, and *d* shells are well described in DFT, whereas interelectronic interactions within the $5f$ shell are treated explicitly. We use the fully anisotropic, rotationally invariant implementation of the $+U$ interaction in the DFT + U method in the full-potential linearized augmented plane wave (FP-LAPW) basis that includes both scalar-relativistic and spin-orbit coupling (SOC) effects [21,22]. The calculations were carried out in the observed paramagnetic state; however, both spin and orbital moment effects, such as rms values of the moments, are included in this U(ED) extension.

The effects of the interaction Hamiltonian $H_{\rm int}$ on the electronic structure are described with the aid of an auxiliary impurity model describing the complete 14-orbital U $5f$ shell. This multiorbital impurity model includes the full Coulomb interaction; the SOC, which is very strong in both U and Te;

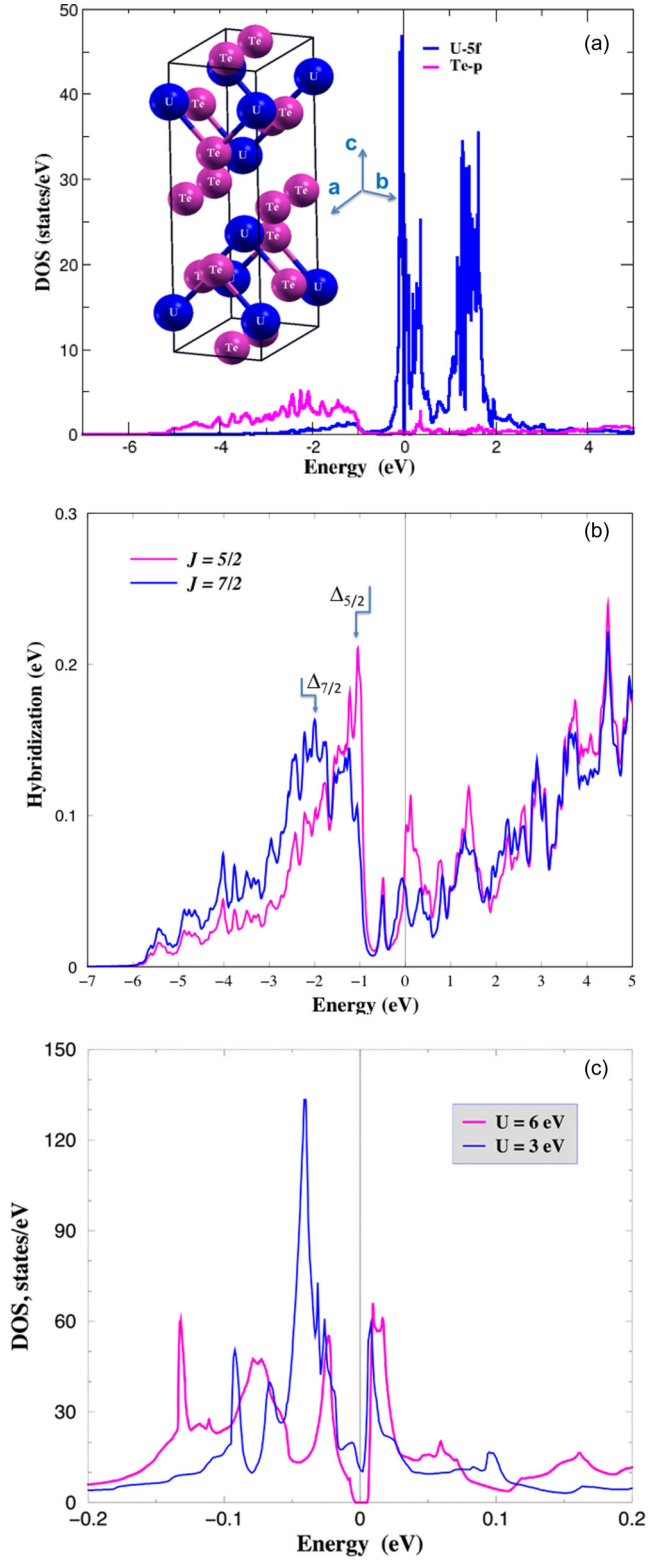

FIG. 1. (a) Projected densities of states/eV (per unit cell) for nonmagnetic UTe_2 from the DFT + U(OP) functional ($U = J =$ 0.5 eV), showing the projections for U $5f$ (blue) and Te $5p$ (magenta). Inset: the orthorhombic *Immm* UTe_2 crystal structure. (b) The $j = \frac{5}{2}$ and $\frac{7}{2}$ projected hybridization functions $\Delta(z) = \frac{1}{\pi n_f} \mathrm{Im\,Tr}[G_0{}^{-1}(z)]$ (eV) obtained from LDA calculations [12]. (c) Total densities of states/eV (per unit cell), for nonmagnetic UTe_2 from the DFT + U(ED) functional. Note that $U = 6$ eV opens a gap.

and the crystal field. The corresponding Hamiltonian can be written (see, for example, Hewson [23])

$$H_{\rm int} = \sum_{\substack{qmm'\\ \sigma\sigma'}} \epsilon^q_{m\sigma,m'\sigma'} b^\dagger_{qm\sigma} b_{qm'\sigma'} + \sum_{m\sigma} \epsilon_f f^\dagger_{m\sigma} f_{m\sigma} + \sum_{mm'\sigma\sigma'} (\xi \mathbf{l}\cdot\mathbf{s} + \Delta_{\rm CF})_{m\sigma,m'\sigma'} f^\dagger_{m\sigma} f_{m'\sigma'} + \sum_{\substack{qmm'\\ \sigma\sigma'}} (V^q_{m\sigma,m'\sigma'} f^\dagger_{m\sigma} b_{qm'\sigma'} + \text{H.c.}) + \frac{1}{2} \sum_{\substack{mm'm''\\ m'''\sigma\sigma'}} U_{mm'm''m'''} f^\dagger_{m\sigma} f^\dagger_{m'\sigma'} f_{m'''\sigma'} f_{m''\sigma}. \quad (1)$$

Here, $f^\dagger_{m\sigma}$ creates an electron in orbital m and spin σ in the $5f$ shell, and $b^\dagger_{m\sigma}$ creates an electron in state $m\sigma$ in the "bath" that consists of those host band states that hybridize with the impurity $5f$ shell. ϵ_f is the energy position of the noninteracting $5f$ "impurity" level, and ϵ^q are the bath energies.

The parameter ξ specifies the strength of SOC obtained from the atomic potential, and $\Delta_{\rm CF}$ is the crystal-field (CF) potential at the impurity, as described below. The matrices V^q describe the hybridization between the $5f$ states and the bath orbitals at energy ϵ^q.

In these calculations, two sets of Slater integrals (in eV),

$$F_0 = 3.00, \quad F_2 = 6.024, \quad F_4 = 4.025, \quad F_6 = 2.94$$

and

$$F_0 = 6.00, \quad F_2 = 6.024, \quad F_4 = 4.025, \quad F_6 = 2.94,$$

were chosen to specify the Coulomb interaction matrix $U_{mm'm''m'''}$ in Eq. (1). They correspond to values of $U = 3$ eV and $U = 6$ eV, respectively, with exchange $J = 0.51$ eV.

C. Computational procedure

1. Overview

The calculation uses the same DFT foundation and interaction matrix as implemented by Shick *et al.* [21] and used in conventional DFT + U calculations, but it generalizes the Shick *et al.* [24] ionic limit approximation ("Hubbard I") to (a) include hybridization with the environment and (b) apply exact diagonalization to evaluate the impurity Green's function, much like some versions of dynamical mean-field theory. A crystal-field potential is included in the formalism, but for UTe_2 it is expected that the DFT treatment of CF is sufficient, as done for other actinides [24].

To specify the bath parameters, we use the previously reported LDA results for nonmagnetic UTe_2 [12] (the conventional basic underlying electronic structure before many-body interaction is considered), repeated for this study. Since the interaction U terms in $H^{\rm int}$ are couched in spin-orbital rather than j, j_z language, it is judicious to treat SOC in $H_{\rm int}$. It is assumed that the first and fourth terms in Eq. (1) are diagonal in $\{j, j_z\}$ representation.

Next, we obtain $V^j_{q=1}$ and $\epsilon^j_{q=1}$, for $j = \frac{5}{2}$ and $\frac{7}{2}$, from the hybridization functions

$$\Delta_j(z) = \frac{1}{\pi n_j} \text{Im Tr}_j\big[G_0{}^{-1}(z)\big], \quad (2)$$

where Tr_j is the trace over the j subspace, with $n_f = 6$ for $j = 5/2$ and $n_f = 8$ for $j = 7/2$. $G_0(z)$ is the noninteracting DFT Green's function extended to the complex energy z plane, equal to the crystal Green's function in Eq. (4) with the self-energy Σ set to zero. The hybridization functions $\Delta_j(\epsilon)$, obtained from the LDA calculation without additional adjustment, are shown in Fig. 1(b). Since the essential hybridization occurs in the energy region of Te p states [see Fig. 1(a)], we set $\epsilon^{5/2}_{q=1}$ to the -1.045 eV peak position of $\Delta^{5/2}(\epsilon)$ and $\epsilon^{7/2}_{q=1}$ to the -1.996 eV peak position of $\Delta^{7/2}(\epsilon)$. From the value of $\Delta(\epsilon_{q=1}) = V^2\delta(\epsilon - \epsilon_{q=1})$, we obtain $V^{5/2}_{q=1} = 0.459$ eV and $V^{7/2}_{q=1} = 0.404$ eV.

2. Local approximation for $\Sigma(z)$

The band Lanczos method [25] is employed to find the lowest-lying eigenstates of the many-body Hamiltonian $H_{\rm imp}$ and to calculate the one-particle Green's matrix $[G_{\rm imp}(z)]_{\gamma,\gamma'}$ in the subspace of the f spin-orbitals $\{\phi_\gamma = \phi_{m\sigma}\}$ at low temperature [$k_{\rm B}T = \beta^{-1} = (1/500)$ eV, T $\sim$ 40 K]. The expression for $G_{\rm imp}$ is

$$[G_{\rm imp}(z)]_{\gamma\gamma'} = \frac{1}{Z} \sum_{\alpha,\delta} \frac{\langle\alpha|c_\gamma|\delta\rangle\langle|\delta|c^\dagger_{\gamma'}|\alpha\rangle}{z + E_\delta - E_\alpha} [e^{-\beta E_\delta} + e^{-\beta E_\alpha}], \quad (3)$$

where Z is the partition function, E_α is the energy of the eigenstate $|\alpha\rangle$ of Eq. (1), and z is the (complex) energy. The self-energy matrix $\Sigma_{\gamma,\gamma'}(z)$ is then obtained from the inverse of the Green's function matrix $G_{\rm imp}$.

The self-energy is then inserted into the local Green's function $G(z)$

$$G_{\gamma\gamma'}(z) = \int_{\rm BZ} \frac{d^3k}{V_{\rm BZ}} [z + \mu - H_{\rm DFT}(\mathbf{k}) - \Sigma(z)]^{-1}_{\gamma\gamma'}, \quad (4)$$

calculated in a single-site approximation as described previously [24,26], from which $5f$ orbital occupations are obtained. $V_{\rm BZ}$ is the volume of the Brillouin zone (BZ). The self-energy is adjusted at each iteration until self-consistency is reached. Since this method has not been used previously, we provide additional details for purposes of clarity in Appendix A, which provides a flowchart and a step-by-step description of the procedure.

3. Density matrix self-consistency

In a single-site approximation, the local Green's function matrix $G(z)$ for the $5f$ electrons in the manifold is

$$G(z) = \big(G_0^{-1} + \Delta\mu - \Sigma(z)\big)^{-1}, \quad (5)$$

where $G_0(z)$ is the noninteracting Green's function and $\Delta\mu$ is a correction to the chemical potential chosen to ensure that $n_f = -\pi^{-1}\text{Im Tr}\int_{-\infty}^{E_F} dz\, G(z)$ is equal to the number of correlated f electrons obtained from Eq. (7). Then, with the aid of

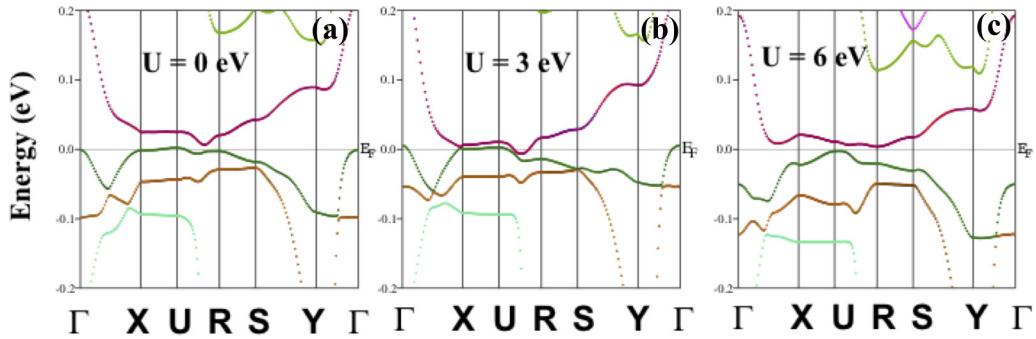

FIG. 2. Band structures near the Fermi level $E_F = 0$ for unpolarized UTe$_2$ from (a) the DFT + U(OP) functional, and from the DFT + U(ED) functional for (b) $U = 3$ eV and (c) $U = 6$ eV. Note that in (b) for $U = 3$ eV, a band crossing at E_F lies very near the point X. The special k points lie along Cartesian directions: Γ $[0, 0, 0]$, X $[\pi/a, 0, 0]$, U $[\pi/a, 0, \pi/c]$, R $[\pi/a, \pi/b, \pi/c]$, S $[\pi/a, \pi/b, 0]$, and Y $[0, \pi/b, 0]$.

this local Green's function $G(z)$, we evaluate the occupation matrix

$$n_{\gamma\gamma'} = -\frac{1}{\pi}\,\mathrm{Im}\int_{-\infty}^{E_F} dz\, G_{\gamma\gamma'}(z). \tag{6}$$

For the energy integrations we use $\Im(z)/\pi = 0.01$ eV and a grid along the real z axis of 0.01 eV.

The matrix $n_{\gamma_1\gamma_2}$ is used to construct an effective LDA+U potential V_U, which is inserted into the Kohn-Sham-like equations [21]:

$$[-\nabla^2 + V_{\mathrm{LDA}}(\mathbf{r}) + V_U + \xi(\mathbf{l}\cdot\mathbf{s})]\Phi_{\mathbf{k}}(\mathbf{r}) = \epsilon^b_{\mathbf{k}}\Phi_{\mathbf{k}}(\mathbf{r}). \tag{7}$$

For the spherically symmetric LDA+U double-counting term (included in the potential V_U) we have adopted the fully localized limit (FLL) form $V_{dc} = U(n_f - 1/2) - J(n_f - 1)/2$. We also note that the LDA potential $\hat{V}_{\mathrm{LDA}}$ in Eq. (7) acting on the f states is corrected to exclude the nonspherical double counting with V_U [26]. The equations in Eq. (7) are iteratively solved until self-consistency over the charge density is reached. The DFT + U Green function matrix G_{+U} is calculated from Eq. (4) substituting the self-energy $\Sigma(\epsilon)$ by the DFT + U potential V_U.

The new value of the $5f$-shell occupation is obtained from the solution of Eq. (7) and defines the new value of $\epsilon_f = -V_{dc}$ in Eq. (1) [24]. The f-shell SOC parameter (an atomic quantity) and the CF matrix Δ_{CF} in Eq. (1) are determined in each iteration. The CF matrix Δ_{CF} in Eq. (1) is obtained by projecting the self-consistent solutions of Eq. (7) into the $\{\phi_\gamma\}$ local f-shell basis, giving the "local Hamiltonian"

$$\begin{aligned}[H_{\mathrm{loc}}]_{\gamma\gamma'} &= \int_{\epsilon_b}^{\epsilon_t} d\epsilon\, \epsilon[N(\epsilon)]_{\gamma\gamma'} \\ &\approx \epsilon_0\delta_{\gamma\gamma'} + [\xi\mathbf{l}\cdot\mathbf{s} + \Delta_{\mathrm{CF}}]_{\gamma\gamma'} + [V_U]_{\gamma\gamma'},\end{aligned} \tag{8}$$

where $[N(\epsilon)]_{\gamma_1\gamma_2}$ is the f-projected density of states (fDOS) matrix (whose integral to E_F gives the familiar occupation matrix), ϵ_b is the bottom of the valence band, ϵ_t is the upper cutoff, and ϵ_0 is the mean position of the noninteracting $5f$ level. The matrix Δ_{CF} is then obtained by removing the interacting DFT + U potential and SOC $[\xi\mathbf{l}\cdot\mathbf{s}]_{\gamma\gamma'}$ from H_{loc} equation (8). As mentioned, for UTe$_2$ it is anticipated that the CF is represented sufficiently by DFT + U, and this step is neglected.

The self-consistency loop is closed by calculating the noninteracting Green's function G_0,

$$G_0(z) = \left(G^{-1}_{+U} + V_U\right)^{-1}, \tag{9}$$

and the next iteration is started by solving Eq. (1) for the updated ϵ_f, ξ, and Δ_{CF} and calculating the new self-energy $\Sigma(z)$. The self-consistent procedure was repeated until the convergence of the $5f$-manifold occupation matrix, with n_f converged to less than 0.01.

III. COMPUTATIONAL RESULTS

The U and Te atoms projected densities of states (DOS) for $U = 3$ eV and the total densities of states for $U = 3$ eV and $U = 6$ eV are shown in Fig. 1. The band structures for two different Coulomb U values are shown in Fig. 2. For all values of U, the DOS near E_F is almost entirely due to U $5f$ states (see Table I). As several groups have noted, there is a small gap for $U = 0$, the curious LDA result.

Increasing U, the two flat bands near E_F become flatter, approach each other, and by $U = 3$ eV become inverted, leaving a band crossing along Γ–X very near X almost exactly at the Fermi level. Increasing U to 6 eV, the bands separate leaving a small 10-meV band gap, again separating disjoint valence and conduction bands. This moving away from E_F of the

TABLE I. The total $N(E_F)$ and f-projected $N_f(E_F)$ densities of states, in eV^{-1}, and the direction-resolved Fermi velocities in units of 10^5 cm/s for $U = 3$ eV. The electric field gradients (EFGs) V_{xx}, V_{yy}, and V_{zz} (subscripts denote second derivatives) are in units of 10^{21} V/m^2, and the dimensionless asymmetry parameter η is given. The two Te sites have EFGs differing by factors of 7–8.

	$N(E_F)$	$N_f(E_F)$	$v_{F,x}$	$v_{F,y}$	$v_{F,z}$
Total	11.04	10.01	0.88	0.64	0.56
FS-1	6.23	5.67	0.48	0.72	0.32
FS-2	4.81	4.34	1.44	0.80	0.80
		Electric field gradient			
Atom	Site	η	V_{zz}	V_{yy}	V_{xx}
U	4i	0.183	13.85	−8.19	−5.66
Te1	4j	0.173	4.56	−2.67	−1.89
Te2	4h	0.176	33.28	−19.56	−13.71

$5f$ bands is qualitatively consistent with DMFT results using $U = 6$ eV. However, we do not obtain any highly dispersive Te $5p$, U $5d$ band in the background, crossing E_F, as in DMFT. In fact, for $U = 6$ eV we obtain again a small gap, whereas (to repeat) UTe_2 is observed to be a heavy-fermion metal, not necessarily in conflict with a semimetal before dynamic correlations are included. Henceforward we focus on our $U = 3$ eV results with flat $5f$ bands crossing E_F.

A. Band structure and Fermi level quantities

Density functional theory with (semi)local exchange-correlation functionals ($U = 0$) gives an insulating band structure for UTe_2, albeit with a very small 10–15-meV gap. Such a gap generally signals a bonding-antibonding separation of bands, but no such description has been forthcoming for UTe_2. The gap reflects a different brand of band insulator. Every calculation reveals that the large uranium SOC separates the $j = \frac{5}{2}$ and $j = \frac{7}{2}$ subshells separated by 1.5 eV (see Fig. 1), and with a $5f^3$ configuration the former subshell is half filled. This SOC separation is much larger than any crystal-field splitting. The previous work of some of the present authors [12] established that with ferromagnetic order imposed, two orbitals, $m_j = \pm\frac{1}{2}$, are half filled and then hybridized, leading to the gap, which is, however, very small. How physical UTe_2 obliterates this gap and in the process emerges as a nearly magnetic but superconducting material is the fundamental issue in the electronic structure of this compound.

Henceforward we focus on $U = 3$ eV results unless otherwise stated, since this value is sufficient to restore a conducting band structure and is typical of values in most uranium intermetallics. From Fig. 2, this "insulator-metal" transition arises from a hybridization reconfiguration of energy levels at the zone boundary points $U = (\frac{\pi}{a}, 0, \frac{\pi}{c})$ and $X = (\frac{\pi}{a}, 0, 0)$. A distinctive feature is that all four bands shown in Fig. 2 are exceedingly flat along $X-U$ (the k_z direction), unlike for $U = 0$ or $U = 6$ eV. Another feature is the band crossing along $\Gamma-X$ very near the point X. The unoccupied band for $U = 6$ eV is nearly dispersionless along the three directions $X-U-R-S$, before mixing with dispersive bands in other regions of the zone.

The values of $N(E_F)$, $N_f(E_F)$, and Fermi velocities along the three crystal axes for $U = 3$ eV are provided in Table I. The Fermi velocities are the rms FS averaged values $v_{F,x} = \sqrt{\langle v^2_{k,xx}\rangle_{\rm FS}}$, and similarly for yy and zz components. The anisotropy is only 10–15%, indicative of three-dimensional conduction; anisotropy is larger for the individual bands. The magnitudes for the separate bands, $0.3–1.4 \times 10^5$ cm/s, indicate very heavy carriers even before renormalization by dynamical processes (electronic and phononic).

From Table I one sees that 90% of $N(E_F)$ is provided by the U $5f$ states. $N(E_F) = 11.0$ states/eV for both spins and per unit cell, for $U = 3$ eV corresponds to a band Sommerfeld constant $\gamma = 13.0$ mJ mol^{-1} K^{-2}. This implies a mass enhancement of nearly 9 from dynamic interactions compared with the experimental value. Note that there is a strong peak in the DOS (up to 59 states/eV) just 10 meV above E_F, corresponding to $\gamma = 70$ mJ mol^{-1} K^{-2}, which is within a factor of 2 of the experimental value of $\gamma = 120$ mJ mol^{-1} K^{-2} [1]. The narrow peak just above E_F implies a strong dependence of properties on stoichiometry.

In materials with large SOC where the $j = \frac{5}{2}$, $j = \frac{7}{2}$ splitting dominates site anisotropy and crystal-field splitting but symmetry is low, state characters are not very transparent. The $|m_l, m_s\rangle$ and $|j, m_j = m_l + m_s\rangle$ decompositions of $N_f(E_F)$ are provided in Appendix B, Table II. The important bit of information is that the $|\frac{5}{2}, \pm\frac{1}{2}\rangle$ components (equal by symmetry) are three times larger than the $|\frac{5}{2}, \pm\frac{5}{2}\rangle$ components and five times larger than the $|\frac{5}{2}, \pm\frac{3}{2}\rangle$ components, with the $m_j = \pm\frac{7}{2}$ components being negligible. These values reflect strong spin-orbital polarization at the Fermi level in UTe_2, which also shows up in the strong anisotropy of the electric field gradients, below.

The Fermi surfaces (FSs) are displayed in the upper panel of Fig. 3. The FSs have three types of sheets: From the lower band are the hole sheet centered at Γ and a fluted hole column along $X-U$, with masses varying by ~50% over the sheets. The second band gives two symmetry-related electron ellipsoids midway between U and R, providing the required charge compensation. The corresponding Fermi velocities, with relative values shown by the color bar in Fig. 3 and mean values provided in Table I, have somewhat less than factor-of-2 anisotropies.

The array of band graphics in the lower part of Fig. 3, presented with flat-band character and plotted along Cartesian directions, provides the relative amounts of the stated spin-orbital characters of bands near the Fermi level. The major contribution to FS-1 along the $X-U$ line arises from $|\frac{5}{2}, \pm\frac{1}{2}\rangle$ orbitals. The Γ-point-centered hole spheroid is more $|\frac{5}{2}, -\frac{5}{2}\rangle$ in character. The electron sheet along $U-R$ arises from a mixture of all three of these orbitals. As in our previous work [12], we find that the Fermi level states are dominated by $|\pm\frac{1}{2}\rangle$ orbitals with some contribution from the $|-\frac{5}{2}\rangle$ orbital.

Our DFT + U(ED) results, obtained without restriction to a single-determinant reference state in determining the density, can be contrasted with previous beyond-DFT results. Admittedly, the groups that are involved are searching for a treatment that will provide a realistic platform for further considerations and experimental properties. Conventional DFT + U was applied by Ishizuka *et al.* [15], who chose the nonstandard Hund's $J = 0$ approach, neglecting Hund's exchange and anisotropy of the $U_{m,m',m'',m'''}$ matrix. A crossover in behavior was found for values of U in the 1–1.5-eV range. Our earlier treatment of orbital polarization by the DFT + U(OP) method [12] focused on ferromagnetic alignment based on the observed large Curie-Weiss moment (which, however, does not order), so it is less directly comparable. The problem posed by the unphysical gap in LDA was addressed by Harima [27] with a hands-on shift of the U $5f$ energy by 1.36 eV, giving small Fermi surfaces arising from flat bands much as we find, and by 2.72 eV, which led to a band structure with large Fermi surfaces. As mentioned, the work of Miao *et al.* [13] was strongly influenced by the apparent similarity of a dispersive band crossing E_F in ARPES that is like that in $ThTe_2$, which has no $5f$ bands.

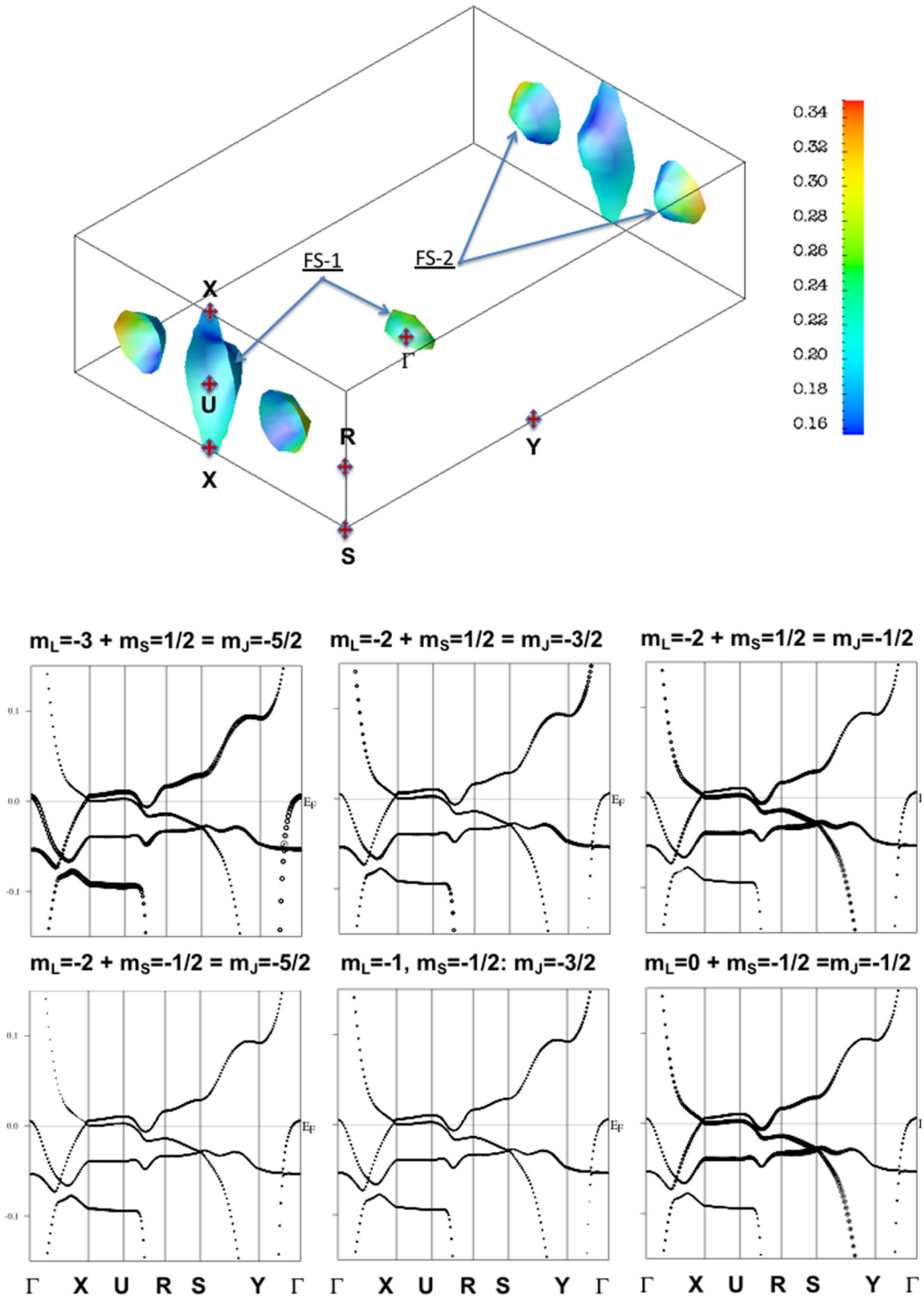

FIG. 3. Upper panel: The Fermi surfaces of UTe_2 from DFT + U(ED), for Coulomb $U = 3$ eV. The colors provide the relative Fermi velocities. The high-symmetry k points are Γ [0,0,0], X $[\pi/a, 0, 0]$, U $[\pi/a, 0, \pi/c]$, R $[\pi/a, \pi/b, \pi/c]$, S $[\pi/a, \pi/b, 0]$, and Y $[0, \pi/b, 0]$. Lower panels: the $5f$ flat-band structure of UTe_2, with the circle size indicating the amount of m_l, m_s, $m_j = m_l + m_s$ character in the bands, as labeled.

B. Local U atom f-shell properties

The calculated $5f$ occupation within the uranium atomic sphere is $n_f = 2.73$, close to the value obtained in DFT + U(OP) calculations [12] and supporting the viewpoint of a reference U $5f^3$ configuration. This value is a slight underestimate, since $5f$ orbitals extend somewhat beyond the atomic spheres used to obtain this number. The electronic structure results discussed above have been more consistent with an f^2 viewpoint, but without the comparison of calculated moments with the experimental Curie-Weiss moment that we provide below.

1. X-ray absorption

X-ray absorption spectroscopy (XAS) provides additional local information. XAS yields two intensities $I_{5/2} : 4d_{5/2} \rightarrow 5f_{5/2,7/2}$ and $I_{7/2} : 4d_{3/2} \rightarrow 5f_{5/2}$, and the branching ratio [28] $B = I_{5/2}/(I_{5/2} + I_{3/2}) = 0.71$. These are connected to the partial occupations $n_f^{5/2} = 2.47$ and $n_f^{7/2} = 0.26$. Our value of B can be directly compared with future experimental results for XAS and electron energy-loss spectroscopies. The $|j, m_j\rangle$ decompositions of the U $5f$ occupations are provided in Appendix B.

2. Curie-Weiss moment

For the self-consistently determined impurity energy position $\epsilon_f = -V_{dc}$, we obtain a doubly (Kramers) degenerate ground state with spin, orbital, and total moments of $S = -1.34$, $L = 5.80$, and $J = 4.53$, in μ_B. The calculated g factor is 0.78, and $\langle m_j \rangle = \pm 0.55$. The Curie-Weiss magnetic moment $\mu_{\text{eff}} = g\sqrt{J(J+1)} = 3.52\ \mu_B$, calculated as the rms value over occupied uranium configurations, is in reasonable agreement with experimental values of 2.8 μ_B [1] and 3.3 μ_B [2]. These can be compared with the textbook values for an f^3 configuration: $S = -\frac{3}{2}$, $L = 6$, and $J = \frac{9}{2}$, resulting in $g = 0.72$. These Hund's rule numbers, not normally reliable for $5f$ materials, are remarkably similar to the DFT + U(ED) results.

3. Mass enhancement

We obtain an estimated average mass enhancement, without contributions from dynamical corrections, in two ways. From the mean spectral density,

$$\frac{m^*}{m} = \frac{\text{Tr}[\hat{Z}^{-1}\hat{N}(E_F)]}{\text{Tr}[\hat{N}(E_F)]},$$

where $\hat{Z}^{-1} = [\hat{I} - d\,\text{Re}[\Sigma(\epsilon)]/d\epsilon]^{-1}$ is the quasiparticle residue matrix and $\hat{N}(E_F) = -\frac{1}{\pi}\,\text{Im}\,\text{Tr}[G(E_F)]$ is the spectral density matrix obtained from Eq. (4). The quasiparticle weight $Z(= \frac{m}{m^*}) = 0.06$ is obtained. This small value of Z indicates the strongly correlated character of f electrons at E_F. The renormalized perturbation theory [23] expression for the Kondo temperature is

$$T_K = \frac{\pi^2}{4} Z \Delta(E_F). \tag{10}$$

From the value of the hybridization function $\Delta(E_F) \approx 50$ meV, the predicted $T_K \approx 100$ K, very similar to experimental values from resistivity [1].

4. Electric field gradients

Electric field gradients (EFGs) provide a measure of the charge distribution (mostly from the local charge) that is available from all-electron calculations. Following the analysis of the electronic structure quantities given above, we have calculated the electric field gradients [29] in UTe_2. Their values, together with the dimensionless asymmetry parameter for the x-y-plane values,

$$\eta = \frac{V_{xx} - V_{yy}}{V_{zz}} \equiv \frac{V_{yy} - V_{xx}}{V_{yy} + V_{xx}},$$

are provided in Table I. The second expression follows from the traceless nature of the EFG tensor. The EFG component V_{zz} is proportional to the nuclear quadrupolar resonance (NQR) frequency ν_Q. Experimental measurements of NQR require stable isotopes with nuclear spin $I \geqslant 1$. No such measurements have been performed to date, so our calculations provide a prediction of this measure of the anisotropy of the charge density and resulting Hartree potential at the nuclei.

The most notable result is that the values for the Te2 site are roughly a factor of 7 larger than for the Te1 site, reflecting a substantially different charge distribution around the two sites. The values for uranium lie midway between, and the anisotropy factors $\eta \approx 0.18$ are the same for all three atomic sites. Measurement of some of these will provide useful information on the electronic density distribution, and orbital polarization, of UTe_2.

IV. COMPARISON BETWEEN BAND STRUCTURE AND PHOTOEMISSION DATA

Comparison of calculated bands (or spectral density) with photoemission spectroscopy (PES) data is the most direct means of determining the basis of the electronic structure. Due to a number of experimental challenges—matrix element effects, energy and k resolution, band broadening due to dynamical effects, and surface sensitivity—comparison can yet leave uncertainty, especially in quantum materials with strong dynamical processes. Angle-integrated averages over the momentum and matrix element dependence, giving the zone-averaged spectral density, provide the most unambiguous information—the spectral distribution of valence band states—on fundamental aspects of the electronic structure. We remind the reader that a band picture provides an optimum set of single-particle characteristics (orbitals and eigenvalues) to best describe ground-state characteristics—energies, charge and spin densities, and quantities derivable from them, for example, EFGs—and by continuity in metals, near ground-state quantities. Single-particle excitations involve self-energies that are minor in many metals but become central in describing heavy-fermion metals. Occupied multiplets and configurations are sampled in the DFT + U(ED) method to determine spin-orbital occupations, while dynamic effects are not included in the band structure we present.

A. AIPES

Data taken at 20 K with $h\nu = 800$ eV photon energy and 120-meV resolution are compared in Fig. 4 with the resolution-broadened DFT + U(ED) DOS; other details of the experiment and analysis are described by Fujimori *et al.* [11]. The unbroadened DOS is shown in Fig. 1. As mentioned above, the most significant region for comparison is at and close below the Fermi energy, where the dynamical self-energy is small. The leading edges at low energy in Fig. 4 are in extremely good experiment-theory agreement. This result is crucial, because DFT + U(ED) displays flat $5f$ bands at and immediately below E_F, whereas both DFT + U [15] and DFT+DMFT [13] displace $5f$ weight away from E_F by several hundred meV for DMFT, or more for DFT + U. This energy shift is much larger than the exper-

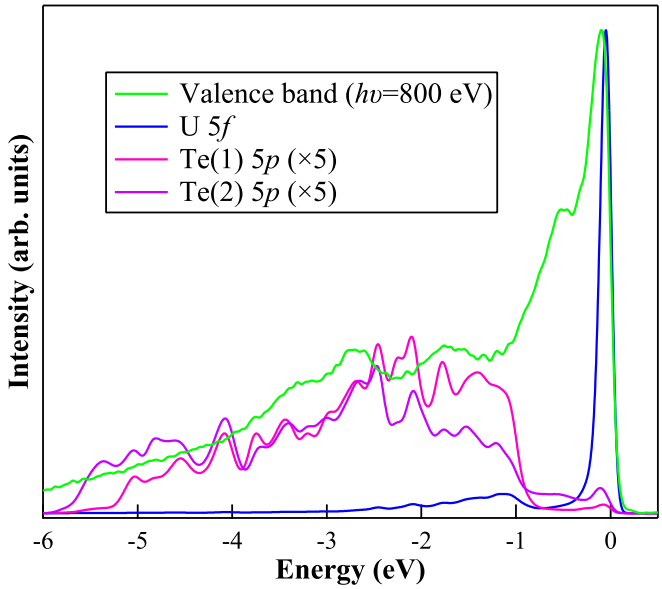

FIG. 4. Measured angle-integrated photoemission spectrum (green) plotted with the resolution-broadened (120-meV Gaussian) and Fermi-Dirac cutoff (20 K) DFT + U(ED) DOS. The agreement of the onsets below E_F reflects flat and heavy bands that become the basis of the heavy-fermion superconductor state. The broadening of the experimental spectrum down to approximately −4 eV is the expected effect of dynamical fluctuations in the uranium 5f shell. The Te DOSs are enhanced by a factor of 5 to reveal possible Te influence on structure in the range of −4 to −1 eV, which is mostly due to single-particle excitations from the 5f shell.

imental resolution, so the corresponding "5f edge" in those spectra should be displaced by this amount from E_F, which is not seen in the data. These AIPES data thus support the view that flat bands lie at E_F, consistent with giving small renormalized Fermi surfaces that provide the platform for the observed exotic superconducting states that are observed to be extraordinarily sensitive to magnetic field, pressure, and stoichiometry.

The AIPES intensity extending to 3–4 eV binding energy can be interpreted in terms of the excitations involving $5f^3$ and $5f^2$ multiplets, as discussed by Miao *et al.* [13]. These considerations involve the relative participations of populations f^2 and f^3. The DFT+DMFT treatment of Miao *et al.* led to a dominant f^2 ($^3H_4$, 84%) state; DFT + U (with U and J values described above) gives exactly f^2 (two strongly bound 5f bands). Our DFT + U(ED) method leads to a dominant f^3 description. Summing the spin-orbital occupations provided in Appendix B (2.73) gives a slight underestimate due to 5f orbital tails extending beyond the sphere boundary. The disjoint valence and conduction bands discussed above argue for a half-filled $j = \frac{5}{2}$ subshell, which is f^3.

B. ARPES

ARPES data were obtained in the photon energy range 565–800 eV with energy resolution of 90–115 meV, with other aspects of the sample and setup described in Ref. [11]. In Fig. 5 we show ARPES results compared with the relevant band lines. For the $U-Z-U$ line shown in Fig. 5(a), agreement between the correlated bands and ARPES data near E_F is apparent, with a dispersive band dropping down at $Z = [0, 0, \pi/c]$ being resolved clearly. For the $X-\Gamma-X$ direction in Fig. 5(b), the calculations yield heavy f bands located near and touching E_F. The bands lie at the same energy as intense emission in the experimental data and are separated by less than the experimental resolution and sometimes crossing, so theory and experiment are consistent although incoherence in the data at this low energy cannot be ruled out. This intensity is at variance with the presence of a light band observed by Miao *et al.* [13] using photon energies in the 30–150-eV range.

Along the $\Gamma-Y-\Gamma'$ line in Fig. 5(c), incoherence in the data lies in the energy region of a dispersive band, apparently reflecting weakly dispersing, largely incoherent, 5f-shell excitations. The strong intensity at [0,0,0] around −60 meV is in a region where our band structure predicts flat 5f bands. Note also that Fig. 5(c) indicates a dispersive Te p band passing through the 5f bands and mixing strongly in the calculations. Thus f-p mixing is substantial, with a result that the Te p character is strongly excluded from the 5f band regions, as is clear from the projected DOS in Fig. 1.

Both the calculated bands near E_F and these data, and also the ARPES data of Ref. [11], differ from the results of Ref. [13]. We attribute the differences in the experimental ARPES data to the higher surface sensitivity of the spectra taken in the 30–150-eV range [13] where the escape depth is ∼8–12 Å. The energy dependence of the electron escape depth [30] indicates that it is roughly twice as large [30] in our energy range. Thus our data are more bulk sensitive, while those of Miao *et al.* [13] are more surface impacted, where confinement imposed by the surface can lead to the U 5f electrons becoming more localized than in the bulk. The low-energy ARPES data of Miao *et al.* were mostly interpreted by the band structure of ThTe$_2$, i.e., without any 5f bands whatsoever. Conversely, our ARPES data together with our correlated band results, along with earlier AIPES data [11], emphasize the presence of heavy 5f bands near E_F.

V. SUMMARY

While a great deal of experimental data have been collected that are relevant to the complex phase diagram of UTe$_2$ and there are several theoretical suggestions about the character and symmetry (or symmetries) of its superconducting and magnetic phases, there is not yet any consensus emerging on its basic electronic structure. Given its heavy-fermion properties, this may not be so surprising, but relative to modestly correlated DFT-based calculations, the dynamical mass enhancement is substantial but not particularly large. The Hill criterion for the critical uranium atom separation [18,19] is 3.5 Å; clearly, UTe$_2$ lies on the localized side of that limit, but it does not order magnetically at zero field. The Hill criterion is, however, sometimes violated in uranium compounds, so the guidance it provides is limited.

There is evidence that neither a fully localized nor a simple itinerant picture holds for UTe$_2$. Our correlated band DFT + U(ED) calculations, motivated by the Anderson impurity model and taking into account the multiconfiguration aspect of the U 5f shell, suggest that both local and itinerant characteristics of the f electrons appear near the Fermi

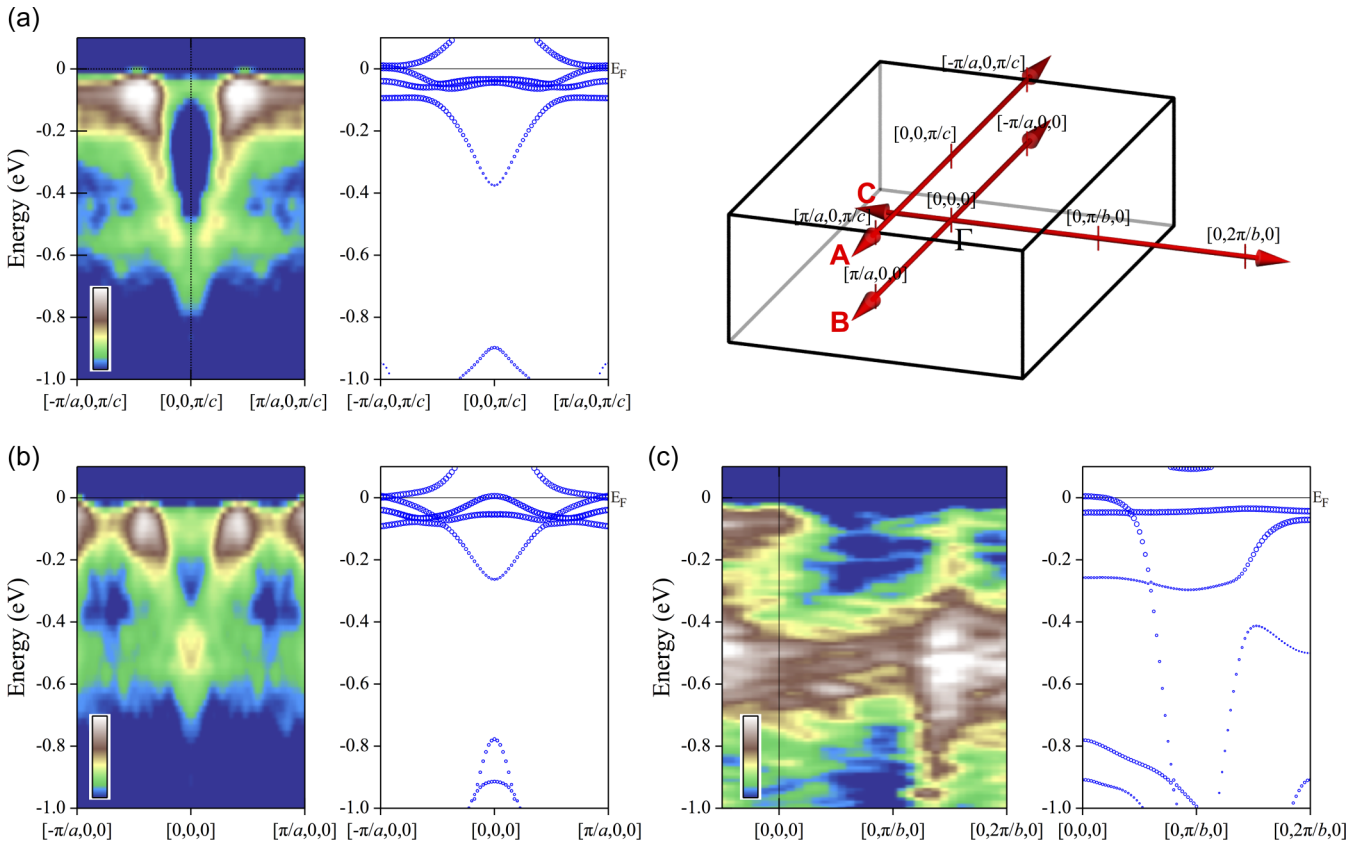

FIG. 5. Upper right panel: Brillouin zone structure of UTe_2. (a)–(c) ARPES spectra (left) together with the band structure (right) for the designated directions and with energies aligned. The size of the calculated points provides the relative amount of $5f$ character of the wave function. (a) and (c) provide new data, while (b) is a replot of earlier data [11] of one of the authors to provide clear comparison with our theoretical results. The k-point notations of the orthorhombic pseudozone Γ $[0, 0, 0]$, X $[\pi/a, 0, 0]$, U $[\pi/a, 0, \pi/c]$, Z $[0, 0, \pi/c]$, Y $[0, \pi/b, 0]$, and Γ' $[0, 2\pi/b, 0]$ are used in the text.

level and need to be treated together. The uranium magnetic moment is given well compared with the two experimental reports, and an unexpected result is that the spin, orbital, and total moments are near the Hund's rule prediction for an f^3 ion, and not representative of an f^2 ion.

The simplest and clearest experimental information on the electronic structure is from angle-integrated PES. The occupied $5f$ spectral density [11] peaks immediately below the Fermi level and is strong within 1 eV of E_F but contains structure (presumably) satellites out to 4 eV binding energy. The measured spectrum represents broadening of a dynamical origin that our method does not take into account. The other two means of including Coulomb repulsion U, DFT + U and DFT+DMFT, both displace the $5f$ spectral density to higher binding energy, leaving only a δ-function-like Kondo peak at E_F (DMFT), not consistent with AIPES data. Our spin-orbital occupations also support dominance of an f^3 ion.

We have compared the DFT + U(ED) bands with the ARPES spectra of Fujimori *et al.* [11] and new data, which used higher photon energy with a larger escape depth and thus more bulk sensitivity than the data of Miao *et al.* [13]. The comparison at low binding energy is encouraging, especially considering some uncertainty in extracting bulk (three-dimensional) band information from emission of electrons through a single surface. For these reasons, we propose that our DFT + U(ED) bands provide an appropriate basis of understanding and building on the electronic structure. We further comment that the flat $5f$ bands crossing E_F lead to small Fermi surfaces that will be responsive to pressure and magnetic field, a sensitivity that is very clear in the emerging experimental phase diagram.

Finally, our low-energy band structure shows evidence of Te $6p$–U $5f$ mixing, which repels the Te $6p$ character from the low-energy region rather than opening up to allow a dispersive Te band to cross the Fermi level. Still, the Te influence is important, and the large U-U separation placing it in the magnetic ion regime suggests that exchange coupling in UTe_2 is primarily of Ruderman-Kittel-Kasuya-Yosida (RKKY) character mediated through the Te conduction bands. The overall picture is one of Fermi level bands dominated by $5f$ character as in UPd_3 versus a more strongly localized moment as in the Kondo lattice picture.

ACKNOWLEDGMENTS

We thank G. R. Stewart for guiding us to the updated uranium Hill plot published in Ref. [19]. A.B.S. acknowledges partial support provided by Operational Programme Research, Development and Education financed by European Structural and Investment Funds and the Czech Ministry of Education, Youth, and Sports (Project No. SOLID21 - CZ.02.1.01/0.0/0.0/16_019/0000760), and by the Czech

TABLE II. The $|m_l, m_s\rangle$ and $|j, m_j\rangle$ decompositions of the U atom f-projected DOS at E_F (in eV^{-1}) are provided for the unpolarized system. The magnetic quantization is along the easy $\hat{a}$ axis; these values are for Coulomb $U = 3$ eV.

m_l	-3	-2	-1	0	1	2	3	
Spin-↑	0.48	0.23	0.85	0.81	0.10	0.07	0.01	
Spin-↓	0.01	0.07	0.10	0.81	0.85	0.23	0.48	
m_j	$-7/2$	$-5/2$	$-3/2$	$-1/2$	1/2	3/2	5/2	7/2
	0.01	0.55	0.33	1.66	1.66	0.33	0.55	0.01

Science Foundation (GACR) Grant No. 18-06240S. The experiment was performed under Proposal No. 2019A3811 at SPring-8 BL23SU. S.-i.F. was financially supported by JSPS KAKENHI Grant Numbers JP16H01084 and JP18K03553. W.E.P. was supported by National Science Foundation Grant DMR 1607139.

APPENDIX A: DENSITY MATRIX SELF-CONSISTENCY IN DFT + U(ED)

The calculation follows in several respects that of Shick *et al.* [24] for their "DFT+Hubbard I approximation" study of elemental actinides. A few generalizations have been adopted here, with the main steps being illustrated in the flow diagram in Fig. 6. The various steps occur in the following order.

(1) From a DFT or LDA calculation, construct the crystal Green's function $G_0(z)$, and choose initial parameters to solve Eq. (1) as reasonable estimates. For example, the repulsion U and Hund's rule J constants (from the Slater parameters) must be specified.

(2) From the (self-consistent) DFT calculation, evaluate the hybridization matrix, from which the bath energies $\epsilon^j_{q=1}$ and hybridization strengths V^j_q are chosen to represent mixing with the environment, as described in Sec. II C. The input parameters to the DFT + U(ED) calculation are now determined.

(3) Carry out an exact diagonalization of $H_{\rm int}$ of Eq. (1). This step is represented by the top panel of the flowchart in Fig. 6. Use eigenvalues and eigenvectors to construct the impurity Green's function $G_{\rm imp}$ in Eq. (3) and the corresponding self-energy; adjust μ in Eq. (5) to fix the value of n_f to the current value from the full calculation equation (7). Calculate the occupation matrix equation (6) as stated in Sec. II C 3.

(4) From the occupation matrix, set up the DFT + U potential, and solve self-consistently the Kohn-Sham equation (7),

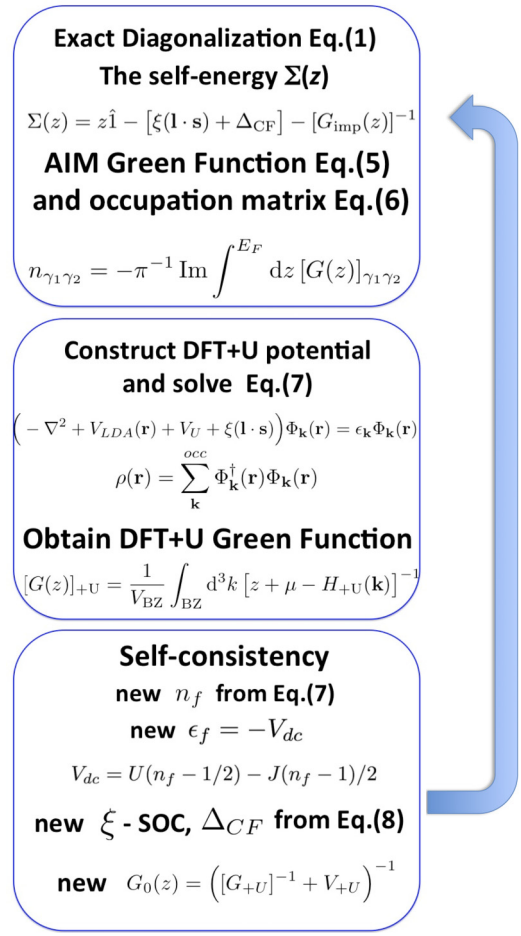

FIG. 6. Flowchart indicating the main steps in the charge and occupation matrix self-consistent procedure for our DFT + U(ED) implementation. See the description in Appendix A. AIM, Anderson impurity model.

to find the updated charge density according to some reliable prescription typically present in DFT codes. Obtain the DFT + U Green's function. See the central panel in Fig. 6.

(5) Obtain a new noninteracting Green's function G_0, a new position ϵ_f of the impurity level, and a new ξ and (when used) $\Delta_{\rm CF}$. This step is represented in the bottom panel in Fig. 6.

(6) Now close the self-consistency loop. When the output and input of the $5f$-manifold occupation n_f convergence agree within a specified criterion, the self-consistency loop is exited, and analysis of the results follows.

TABLE III. The $|j, m_j\rangle$ decompositions of the U atom f occupation for the unpolarized system. The magnetic quantization is along the easy $\hat{a}$ axis. Coulomb $U = 3$ eV and $U = 6$ eV values are provided.

j \ mj	$-7/2$	$-5/2$	$-3/2$	$-1/2$	1/2	3/2	5/2	7/2
				$U = 3$ eV				
5/2		0.412	0.410	0.415	0.415	0.410	0.412	
7/2	0.031	0.037	0.031	0.030	0.030	0.031	0.037	0.031
				$U = 6$ eV				
5/2		0.410	0.417	0.410	0.410	0.417	0.410	
7/2	0.027	0.019	0.033	0.022	0.022	0.033	0.019	0.027

APPENDIX B: DECOMPOSITION OF THE U 5f DOS AT E_F, AND THE U 5f OCCUPATIONS

The essential aspects of the electronic structure of UTe_2 finally reduce to participation of various spin-orbitals in the 5f occupation and to their play in states at the Fermi level. Table II provides the Fermi level quantities in both (ℓ, s) and (j, m_j) representations. The primary result to notice is the large and equal participation at E_F of the $m_j = \pm\frac{1}{2}$ orbitals.

Table III provides the strong spin-orbit decompositions for moment along the easy $\hat{a}$ axis. The $j = \frac{7}{2}$ contribution is minor.

[1] S. Ran, C. Eckberg, Q.-P. Ding, Y. Furukawa, T. Metz, S. R. Saha, I.-L. Liu, M. Zic, H. Kim, J. Paglione, and N. P. Butch, Nearly ferromagnetic spin-triplet superconductivity, Science **365**, 684 (2019).

[2] D. Aoki, A. Nakamura, F. Honda, D. Li, Y. Homma, Y. Shimizu, Y. J. Sato, G. Knebel, J.-P. Brison, A. Pourret, D. Braithwaite, G. Lapertot, Q. Niu, M. Valiska, H. Harima, and J. Flouquet, Unconventional superconductivity in heavy fermion UTe_2, J. Phys. Soc. Jpn. **88**, 043702 (2019).

[3] S. Ikeda, H. Sakai, D. Aoki, Y. Homma, E. Yamamoto, A. Nakamura, Y. Shiokawa, Y. Haga, and Y. Onuki, Single crystal growth and magnetic properties of UTe_2, J. Phys. Soc. Jpn. **75**, 116 (2006).

[4] Y. Tokunaga, H. Sakai, S. Kambe, T. Hattori, N. Higa, G. Nakamine, S. Kitagawa, K. Ishida, A. Nakamura, Y. Shimizu, Y. Homma, D. Li, F. Honda, and D. Aoki, ^{125}Te-NMR study on a single crystal of heavy fermion superconductor UTe_2, J. Phys. Soc. Jpn. **88**, 073701 (2019).

[5] S. Ran, C. Eckberg, Q.-P. Ding, Y. Furukawa, T. Metz, S. R. Saha, I-L. Liu, M. Zic, H. Kim, J. Paglione, and N. P. Butch, Spontaneously polarized half-gapped superconductivity, arXiv:1811.11808.

[6] T. Metz, S. Bae, S. Ran, I.-L. Liu, Y. S. Eo, W. T. Fuhrman, D. F. Agterberg, S. Anlage, N. P. Butch, and J. Paglione, Point node gap structure of spin-triplet superconductor UTe_2, Phys. Rev. B **100**, 220504(R) (2019).

[7] D. Aoki, K. Ishida, and J. Flouquet, Review of U-based ferromagnetic superconductors: Comparison between UGe_2, URhGe, and UCoGe, J. Phys. Soc. Jpn. **88**, 022001 (2019).

[8] C. S. Wang, M. R. Norman, R. C. Albers, A. M. Boring, W. E. Pickett, H. Krakauer, and N. E. Christensen, Fermi surface of UPt_3 within the local-density approximation, Phys. Rev. B **35**, 7260 (1987).

[9] G. J. McMullan, P. M. C. Rourke, M. R. Norman, A. D. Huxley, N. Doiron-Leyraud, J. Flouquet, G. G. Lonzarich, A. McCollam, and S. R. Julian, The Fermi surface and f-valence electron count of UPt_3, New J. Phys. **10**, 053029 (2008).

[10] T. Oguchi and A. J. Freeman, Hybridization, electronic structure and properties of uranium intermetallics: URu_3, URh_3, UPd_3, UIr_3 and UPt_3, J. Magn. Magn. Mater. **61**, 233 (1986).

[11] S.-I. Fujimori, I. Kawasaki, Y. Takeda, H. Yamagami, A. Nakamura, Y. Homma, and D. Aoki, Electronic structure of UTe_2 studied by photoelectron spectroscopy, J. Phys. Soc. Jpn. **88**, 103701 (2019).

[12] A. B. Shick and W. E. Pickett, Spin-orbit coupling induced degeneracy in the anisotropic unconventional superconductor UTe_2, Phys. Rev. B **100**, 134502 (2019).

[13] L. Miao, S. Liu, Y. Xu, E. C. Kotta, C.-J. Kang, S. Ran, J. P. Paglione, G. Kotliar, N. P. Butch, J. D. Denlinger, and L. A. Wray, Low Energy Band Structure and Symmetries of UTe_2 from Angle-Resolved Photoemission Spectroscopy, Phys. Rev. Lett. **124**, 076401 (2020).

[14] Y. Xu, Y. Sheng, and Y.-F. Yang, Quasi-Two-Dimensional Fermi Surfaces and Unitary Spin-Triplet Pairing in the Heavy Fermion Superconductor UTe_2, Phys. Rev. Lett. **123**, 217002 (2019).

[15] J. Ishizuka, S. Sumita, A. Daido, and Y. Yanese, Insulator-Metal Transition and Topological Superconductivity in UTe_2 from a First-Principles Calculation, Phys. Rev. Lett. **123**, 217001 (2019).

[16] S.-I. Fujimori, I. Kawasaki, Y. Takeda, H. Yamagami, A. Nakamura, Y. Homma, and D. Aoki, Core-level photoelectron spectroscopy of UTe_2, J. Phys. Soc. Jpn. **90**, 015002 (2021).

[17] G. Zwicknagl, 5f electrons in actinides: dual nature and photoemission spectra, Int. J. Mod. Phys. B **21**, 2232 (2007).

[18] H. H. Hill, The early actinides: the periodic system's f electron transition metal series, in *Plutonium 1970 and Other Actinides*, edited by W. N. Miner (Metallurgical Society of the AIME, New York, 1970), p. 2.

[19] A. M. Boring and J. L. Smith, Plutonium condensed matter physics: A survey of theory and experiment, Los Alamos Sci. **26**, 90 (2000).

[20] E. R. Ylvisaker, W. E. Pickett, and K. Koepernik, Anisotropy and magnetism in the LSDA + U method, Phys. Rev. B **79**, 035103 (2009).

[21] A. B. Shick, A. I. Liechtenstein, and W. E. Pickett, Implementation of the LDA+U method using the full-potential linearized augmented plane-wave basis, Phys. Rev. B **60**, 10763 (1999).

[22] A. B. Shick and W. E. Pickett, Magnetism, Spin-Orbit Coupling, and Superconducting Pairing in UGe_2, Phys. Rev. Lett. **86**, 300 (2001).

[23] A. Hewson, *The Kondo Problem to Heavy Fermions* (Cambridge University Press, Cambridge, 1993).

[24] A. B. Shick, J. Kolorenc, A. I. Lichtenstein, and L. Havela, Electronic structure and spectral properties of Am, Cm, and Bk: Charge-density self-consistent LDA + HIA calculations in the FP-LAPW basis, Phys. Rev. B **80**, 085106 (2009).

[25] J. Kolorenc, A. Poteryaev, and A. I. Lichtenstein, Valence-band satellite in ferromagnetic nickel: LDA+DMFT study with exact diagonalization, Phys. Rev. B **85**, 235136 (2012).

[26] O. Kristanovski, A. B. Shick, F. Lechermann, and A. I. Lichtenstein, Role of nonspherical double counting in DFT+DMFT: Total energy and structural optimization of pnictide superconductors, Phys. Rev. B **97**, 201116(R) (2018).

[27] H. Harima, How to obtain Fermi surfaces of UTe_2, JPS Conf. Proc. **29**, 011006 (2020).

[28] K. T. Moore and G. van der Laan, Nature of the 5f states in actinide metals, Rev. Mod. Phys. **81**, 235 (2009).

[29] P. Mohn, Theoretical aspects of hyperfine interactions, Hyperfine Interact. **128**, 67 (2000).

[30] A. Damascelli, Probing the electronic structure of complex systems by ARPES, Phys. Scr. **T109**, 61 (2004).